Journal of Catalysis 410 (2022) 221–235

Contents lists available at ScienceDirect

Journal of Catalysis

journal homepage: www.elsevier.com/locate/jcat

Effects of the method of active site characterization for determining structure-sensitivity in Ag-catalyzed ethylene epoxidation

Benjamin T. Egelske [a,1], Wen Xiong [b,1], Haiying Zhou [c], John R. Monnier [c,*]

[a] Applied Catalysts, Laurens, SC, United States
[b] Micromeritics Instrument Corporation, Norcross, GA, United States
[c] Department of Chemical Engineering, University of South Carolina, Columbia, SC, United States

ARTICLE INFO

Article history:
Received 31 January 2022
Revised 18 March 2022
Accepted 21 March 2022
Available online 6 April 2022

Keywords:
Ethylene oxide
Selectivity
Silver particle size
Turnover frequency
Chemisorption

ABSTRACT

Catalysts have been prepared on a low surface area α-Al_2O_3 support used commercially for previous generation olefin epoxidation catalysts. Prescreening of the low surface area alumina (0.73 m^2/g) indicated the absence of acid catalyzed isomerization of EO at an evaluation temperature of 210 °C. A 0.1 wt% Ag base material synthesized by incipient wetness impregnation of $AgNO_3$ was used as a base material for electroless deposition (ED) of additional Ag to increase particle sizes by controlled reduction of Ag^+ directly onto the preexisting Ag surface to form weight loadings between 0.3 and 5.0 wt% metal. A 12 wt% Ag/α-Al_2O_3 using $Ag_2C_2O_4$ as the Ag precursor was also prepared to compare performance of the ED samples with a catalyst more typical of industrial formulations. Characterization by SEM, STEM, and hydrogen titration of oxygen precovered Ag characterized before and after catalytic evaluation indicated that microscopy is required to accurately represent distributions of Ag particle sizes, but H_2 titration of O-precovered Ag gives the best representation of active sites since it directly counts the number of Ag surface sites. Larger particles >100 nm are resistant to both Ag sintering and carbon foulant; TOF values were relatively insensitive to particle size with only a 2.2 × difference between the best and worst performing samples. Selectivity, which is not a function of TOF, shows the most significant structure sensitivity effect where particle sizes follow the trend 67 nm ≈ 92 nm (58% EO) < 157 nm (67% EO) < 211–542 nm (73% EO). The lower EO selectivities were also correlated with increased fouling for the smaller Ag sizes, suggesting that more strongly bound EO precursor(s) leads to combustion and CO_2/H_2O formation.

1. Introduction

Ethylene Oxide (EO) is currently a 35 M metric ton/year chemical that is expected to continue to grow at a 5–7% annual growth rate for the foreseeable future [1]. This is a remarkably healthy growth rate, particularly for a mature chemical like EO. Several billion lbs of additional capacity have recently been added in the Texas and Louisiana gulf coast due to the supply of cheap ethylene from cracking of natural gas [2]. It is the largest volume product prepared by a heterogeneously-catalyzed oxidation process [3] and accounts for almost 50% of the volume of all oxidation products. Modern high-performance catalysts no longer resemble the unpromoted Ag catalyst disclosed by Lefort in 1933 [4]. Catalyst developments to improve selectivity to EO have gone through several phases as recently detailed [5]. Chronologically, Cs-promoted, Ag catalyst boosted selectivity to the 80% level and then further by the addition of Re^{+7} and other high valent salts including Mo^{+6}, W^{+6}, S^{+6} existing as high valent oxyanions as described by Lauritzen [6,7] EO selectivities are now as high as 90–92% for initial time on-line periods. Because the active Ag surface is loaded with multiple promoters to boost selectivity, the Ag surface site concentrations are often too low for acceptable space time yields, forcing Ag weight loadings to be increased to 30–40 wt% on non-acidic, fused α-Al_2O_3 supports. These supports typically have surface areas <1 m^2/g. The scanning electron micrograph (SEM) in Fig. 1 illustrates the variety of Ag particle sizes for "only" 12 wt% Ag supported on an older generation of α-Al_2O_3 rings with a surface area of 0.73 m^2/g, determined in our laboratory using Kr BET surface area analysis. The Ag is shown as white particles on the dark gray α-Al_2O_3 surface with a wide distribution of Ag particle sizes and the presence of different morphologies including triangles,

* Corresponding author.
E-mail addresses: ben.egelske@appliedcatalysts.com (B.T. Egelske), wen.xiong@micromeritics.com (W. Xiong), hzhou@email.sc.edu (H. Zhou), monnier@cec.sc.edu (J.R. Monnier).
[1] Co-first author.

https://doi.org/10.1016/j.jcat.2022.03.021
0021-9517/

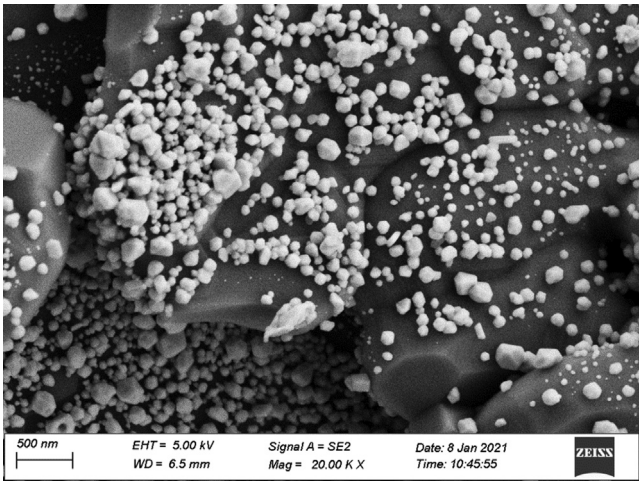

Fig. 1. 12 wt% Ag supported on SA5562 alpha alumina. This sample was prepared from silver oxalate ($Ag_2C_2O_4$) according to reference [22]. Note the wide distribution Ag particle size and the presence of different morphologies including triangles, spheres, and faceted cuboctahedra.

spheres, and faceted cuboctahedrons (Ag is an fcc metal). Even at 20,000× magnification, the α-Al_2O_3 surface appears rather featureless and not likely to anchor Ag particles as well as higher surface area and more interactive supports. However, to achieve the low acidity required to maintain the epoxide ring structure, low surface areas are basic requirements of all catalyst supports used for ethylene epoxidation; α-Al_2O_3 supports with low Bronsted and Lewis acidities [8,9] are preferentially used for the Ag particles.

One of the obvious questions that has not been clearly resolved is whether ethylene epoxidation is a structure-sensitive reaction; that is, does the rate of reaction per Ag site, more commonly known as the turnover frequency (TOF), change with the Ag particle size. It is not possible to answer this question if Ag particle sizes exist over a wide range as in Fig. 1, since reaction rates are the sum of all particle sizes. Likewise, it is critical to have an accurate way to measure active Ag surface site concentrations. Monnier showed in earlier work [10] that a comparison of four typical techniques to measure Pt surface site concentrations of a PEM fuel cell, specifically selective chemisorption (pulsed H_2 titration of oxygen precoved Pt), electrochemical surface area (ESA), x-ray line broadening, and electron microscopy, by far the two preferred methods were selective chemisorption and ESA because they actually measured, or counted, either H_2 molecules or electrons, respectively. X-ray line broadening worked only until XRD peaks became too narrow and insensitive to reflect further changes crystallite size. Of course, the problem with electron microscopic methods is the small number of particles actually measured and whether they represent the entire surface.

Regardless, structure-sensitivity on α-Al_2O_3 supports has been investigated by a number of groups whose particle size determinations are shown in Table 1. Ag particle sizes were determined by both chemisorption and particle counting of microcopy images. In some cases, the numbers of particles countered were <200, and in all cases <500. It was also not stated whether the observed size distributions were assumed to be representative of the entire sample and whether the distribution was assumed for the full Ag weight loading to determine the Ag site concentrations for spherical or hemispherical (same result) particles.

In earlier work, Monnier [11] used SEM measurements and automated particle counting software to count many more particles (n = 17,500 particles) to determine a well-defined distribution of particle sizes. This size distribution shown in Fig. 2 is not from this study but has been added to illustrate that for catalysts with a wide range of particle sizes, large numbers of particles must be measured and counted to obtain accurate particle sizes from which the concentration of active sites can be determined.

The distribution in Fig. 2 was applied to the entire 13.4% Ag loading to calculate the Ag site concentration for each "bin" of particle sizes. The results indicated that after measurement of Ag particles by SEM and summation of all Ag particles, there were 4.0×10^{13} Ag particles/g catalyst having 8.1×10^{18} Ag surface sites/g-cat, and a corresponding surface area average Ag particle size of 0.11 μm calculated from the definition of Ag dispersion where Disp = n_s/n_t, n_s = total number of Ag surface sites (8.1×10^{18}/g-cat) and n_t = total number of Ag atoms in 13.4 wt% Ag (7.5×10^{20}/g-cat). Dispersion can also be described as $n_s = \sum(4\pi r^2)/8.7$ Å^2 and $n_t = \sum(4/3\ \pi r^3/17.1$ Å^3, where r is the radius (in Å) of a Ag particle; this formalism reduces to Ag dispersion = 5.7/r (in Å). The values of 8.7 Å^2 and 17.1 Å^3 refer to the projected surface area of a Ag surface atom and volume of a Ag atom in an fcc lattice, respectively [10]. Thus, for a dispersion of 0.011 and application of disp = 5.7/r (in Å), the average Ag particle size from SEM images was estimated to be ~0.10 μm. Note, however, that >17,000 particles were measured to obtain this value.

For instances where chemisorption has been reported, the data are typically based on dissociative O_2 adsorption and use 1 Ag to ½ O_2 stoichiometry. Both O_2 chemisorption and H_2 titration of O precovered Ag sites have been used by Vannice but results were shown to be more consistent with H_2 titration [12] where the only species capable of undergoing reaction with H_2 to form H_2O was monoatomic oxygen bound to the Ag surface [13]. While there are possibly and likely more than metallic Ag sites capable of adsorbing atomic oxygen, particularly for current generation, heavily promoted Ag catalysts containing Cs, Re, Mo, W, S after a high temperature reduction treatment, only Ag-O species are reactive for H_2 titration at 170 °C. The high valencies of Re and its co-promoters and the very low ionization potential of Cs_2O (or CsOH) make it difficult for reduction by H_2 at temperatures such as 170 °C. This work will be discussed in more detail in a soon to be published paper [14]. Further, the 1:1 H_2 to Ag-O stoichiometry doubles the sensitivity of detection improving sample-to-sample repeatability specifically for systems with low Ag site concentrations such as EO catalysts with large particle sizes.

Many have examined the EO reaction for structure sensitivity but problems exist not only for sensitive and accurate methods of measuring Ag active sites, but also the preparation of catalysts with narrow particle size distribution. The listing of some of the more recent studies is shown in Table 1. Verykios [15] prepared Ag particle sizes between 35 and 170 nm using four different α-Al_2O_3 supports with surface areas ranging from 0.2 to 3.0 m^2/g. Samples were characterized by selective oxygen chemisorption at 200 °C and evaluated between 180 and 240 °C at 220 psig in an oxygen-rich feed. For one series, EO selectivities decreased as Ag particles increased from 120 to 170 nm diameter; however, with a different α-Al_2O_3, selectivity increased as particles grew from 50 to 130 nm [15]. In later work Verykios, Pitchai, and Lee re-examined Ag particle size effects for a wide range of oxide supports and found that most of the oxides strongly contributed to the rate of combustion with only SiO_2 and α-Al_2O_3 having significant selectivity for EO formation [16]. Contrary to the prior work where a minimum in EO formation rate was identified at 70 nm [15], the α-Al_2O_3 supported samples in this study exhibited a maximum rate of formation between 40 and 80 nm [16]. Danilyuk et al later noted the difficulty of obtaining tight particle size distributions on low surface area α-Al_2O_3. Even using a higher surface area of 7 m^2/g for alumina prepared in their laboratory which should help in narrowing particle size distributions, Ag particles between 19 and 140 nm were formed by incipient wetness. Ag particle sizes

Table 1
Literature reported Ag particle size and preparation parameters for epoxidation catalysts supported on α-Al_2O_3.

Ref	Ag precursor	α-Al_2O_3 support	Synthesis	SA (m^2/g)	Ag (wt %)	Max synthesis temperature (°C)	Fresh $size_{chemi}$ (nm)	Fresh $size_{TEM}$ (nm)	No. of particles counted
[15]	$AgNO_3$	MAG-99	Note E	0.2	1	200	36	–	–
				0.2	1	400	43	–	–
				0.2	1	480	47	–	–
				0.2	1	600	53	–	–
				0.2	1	750	59	–	–
		Norton SA-5202		0.63	13.9	200	120	–	–
				0.63	13.9	400	141	–	–
				0.63	13.9	500	166	–	–
		Carborundum SAH7-99-Series		0.97	5.6	200	55	–	–
				0.97	5.6	400	70	–	–
				0.97	5.6	500	78	–	–
				0.97	5.6	600	100	–	–
				0.97	5.6	700	121	–	–
		Prepared by Authors		3.03	6.4	200	31	–	–
				3.03	6.4	410	43	–	–
				3.03	6.4	510	75	–	–
				3.03	6.4	700	108	–	–
				3.03	6.4	850	123	–	–
[16]	$AgNO_3$	Source Not Specified	Note D	0.5	0.5	200	13	10	100–200
				0.5	1	200	26	20	100–200
				0.5	2	200	41	35	100–200
				0.5	5	200	80	78	100–200
				0.5	10	200	100	88	100–200
[23]	Ag Amine in Ethanolamine	Prepared by Authors	Note A	7	0.4	240	13	16 ± 9	100
				7	0.6	240	–	20	–
				7	1.5	240	–	24.3	–
				7	2.4	240	20	18.4	–
				7	2.7	240	30	30.6	–
				7	3.7	240	25	40	–
				7	5.2	240	–	56	–
				7	6.5	240	56	45	–
				7	13.8	240	126	100 ± 32	100
[18]	$Ag_2C_2O_4$	BASF AL4196E	Note C, H_2	8	15	215	–	28 ± 19	170
			Note C, N_2	8	15	215	–	62 ± 21	105
			Note C, O_2	8	15	215	–	76 ± 37	104
[19]	$Ag_2C_2O_4$	Saint-Gobain NorPro SA 5102	Note B He/O_2 (100/0)	1.04	1.3	400	–	19 ± 9	200
				1.04	1.7	275	–	23 ± 11	400
				1.04	4.5	275	–	41 ± 16	400
			Note B He/O_2 (90/10)	1.04	1.7	275	–	48 ± 19	400
				1.04	4	275	–	57 ± 21	400
				1.04	8.7	275	–	99 ± 32	400
				1.04	8.2	275	–	106 ± 47	199
				1.04	10	275	–	127 ± 47	349
			Note B He/O_2 (90/10)	1.04	7.8	500	–	167 ± 58	291
				1.04	14.4	275	–	183 ± 89	484

A. Incipient Wetness → Contact Drying (25 °C) → Vacuum Reduction (90 °C) → Water Wash → Dry in Static Air (100 °C) → Calcination (240 °C, 2 h) [23].
B. Incipient Wetness → Vacuum Drying (25 °C, 1 h) → Calcination in He/O_2 (275, 400, or 500 °C, 10 °C/min, 4 h) [19].
C. Incipient Wetness → Drying in Static Air (60 °C, 24 h) → Heating in H_2, O_2, or N_2 (215 °C, 5 °C/min, 2 h) [18].
D. Incipient Wetness → Atmospheric Drying (70 °C) → H_2 Reduction (200 °C, 6 h) [16].
E. Incipient Wetness → Atmospheric Drying (50 °C) → Water Wash → Atmospheric Drying (50 °C) → H_2 Reduction (200 °C, 60 h) → N_2 Sintering (6–70 h) [15].
F. Prepared by impregnation of Ag oxalate and fast calcined in high velocity air at 260 °C [22].
G. The fresh notation indicates that the sample was reduced or calcined but was not exposed to epoxidation conditions.

were determined by TEM imaging of approximately 100 particles and compared with oxygen chemisorption whose experimental parameters were referenced in earlier work [17]. Evaluation for a C_2H_4-lean feed containing 2% C_2H_4, 7% O_2, balance N_2 at 230 °C and 14.7 psia pressure gave a linear increase in the rate of EO formation with increasing Ag particle size over the range 19–140 nm; selectivity values were not discussed. In 2017 de Jongh [18] examined the effect of gas compositions on precursor decomposition for Ag particle sizes during preparation of 15 wt% Ag samples supported on 8.0 m^2/g α-Al_2O_3. Particle size measurements were determined using a combination of TEM and SEM for 100–170 particles per sample. These results were supplemented with UV/Vis spectra to examine the Ag plasmon peak positions in the 300–750 nm range to infer Ag particle diameters assuming spherical geometry. Catalyst evaluation was conducted in a C_2H_4-rich feed and the authors concluded that at constant C_2H_4 conversions of ~2.8%, the EO selectivity of approximately 50% was independent of Ag particle sizes over the range ~20–400 nm. However, in the analysis it was assumed that selectivity was dependent only on the competitive rates of epoxidation versus C_2H_4 combustion and that the rate of sequential EO combustion was negligible and independent of the temperature used to reach 2.8% C_2H_4 conversion. However, the higher surface area of the α-Al_2O_3 favors existence of some amount of Lewis or Bronsted acidity that may result in some isomerization of EO to acetaldehyde which will rapidly undergo combustion; thus, the assumption that sequential com-

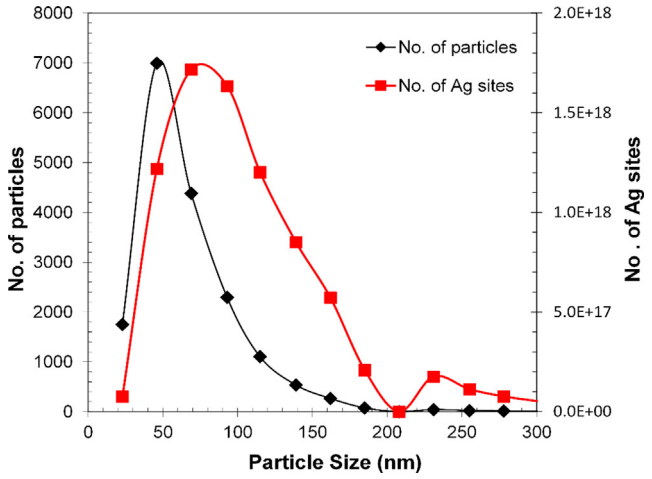

Fig. 2. Particle size distribution generated from 17,500 particles for a 13.4 wt% Ag/α-Al_2O_3 catalyst. The difficulty of conventional approaches based on SEM data is that site concentrations for a particular particle size may not represent the actual quantity of particles for a given size range.

bustion of EO does not occur may be faulty. Recently, Hoof et al studied a series samples supported on 1.04 m^2/g α-Al_2O_3 with loadings between 1.7 and 14.0 wt% Ag. Particle sizes between 20 and 185 nm were determined from Scanning Transmission Electron microscopy (STEM) for 200–485 particles per sample [19]. For an oxygen-rich feed (10% O_2, 5% C_2H_4, balance He at 225 °C and 290 psig) it was concluded that O_2 dissociation does not occur on the external Ag surface and instead only proceeds at defect sites to form subsurface monatomic oxygen which is the responsible species for selective epoxidation. The authors stated that there was a theoretical maximum of EO selectivity of 75% for particles <100 nm and 80% for Ag particles >100 nm as C_2H_4 conversion approached 0%. In summary, there have been no agreement in activity or selectivity trends, likely because of the methods used to measure Ag particle sizes, methods of catalyst preparation, feed compositions, and the variety of supports that have been used.

Thus, in this communication, we prepare a series of supported Ag catalysts using our method of electroless deposition (ED) [20] to deposit Ag on pre-existing Ag nuclei prepared by dry impregnation of 0.1 wt% Ag/α-Al_2O_3 to give better control of resulting Ag particles. We also use an older generation, high purity and low surface area α-Al_2O_3 support (St Gobain, SA-5562) that has been used commercially in older generation EO catalysts. The extruded into ¼" rings were ground and sieved to 841–400 μm (20/40 mesh) before Ag was deposited. Interestingly, this ED process is much like development of silver halide photographic films where Ag particles of 2–6 atoms (called latent images) produced by the photoreduction of AgCl during light exposure were reduced further (by unexposed AgCl particles adjacent to the latent image) during film development by a formaldehyde-containing developer solution to form a negative film [21]. In this study we also use formaldehyde as the reducing agent in the ED bath and $AgNO_3$ as the reducible Ag salt. The principal difference here is we begin with ultra-small Ag particles prepared by dry impregnation.

Ag particles have been analyzed by H_2 titration of oxygen-precovered Ag surface sites at 170 °C using the method developed by Vannice [13] to measure Ag surface site concentrations and compared to SEM micrographs which determine Ag particle size distributions but only infer Ag active site concentrations. The catalysts have been evaluated using an automated reactor system operating at reaction conditions similar to those used industrially, i.e., 210 °C, 250 psig of 8% O_2, 25% C_2H_4, and balance CH_4. The only exception is that no ethyl chloride (EtCl) was not added to the feed to remove the uncertainty of chlorination of Ag. By knowing the number of active surface Ag sites and accurately measuring reaction rates and EO selectivities, it should be possible to determine with substantial accuracy whether ethylene epoxidation is structure sensitive and if EO selectivity has an optimum Ag size range. Finally, the TOF's in this manuscript are reported for site concentrations determined before and after 150 h or more of reaction time to measure steady state activities and to determine sintering characteristics of different Ag particle sizes on the α-Al_2O_3 support.

2. Experimental

2.1. Catalyst preparation

The 0.1 wt% Ag base catalyst was prepared by wet impregnation of $AgNO_3$ (Alpha Aesar) dissolved in deionized water on fused α-Al_2O_3 rings, provided by St Gobain (denoted as SA5562.) Fig. 3 shows Hg intrusion data, illustrating a bimodal macro-pore distribution at 1 and 30 μm in diameter. For supports such as these, internal diffusion limitations are largely nonexistent.

After impregnation of 0.1 wt% $AgNO_3$ on 20/40 mesh SA5562, the sample was transferred to a 400 ml round bottom flask and tumble dried at 10 in of Hg pressure at 70 °C until free tumbling of the support was observed. Samples were transferred to a vacuum oven (VWR Model 1410) at 20 in Hg pressure and heated to 110 °C for 12 h prior to reduction in 125 SCCM of 50% H_2/balance He at 200 °C (ramp rate 5 °C/min) for 4 h in a vertical, split tube furnace. All temperatures used in this study were maintained at ≤210 °C to minimize sintering of Ag particles. The comparison sample of 12 wt% Ag was prepared by impregnation using $Ag_2C_2O_4$ (silver oxalate) as previously noted [22].

The 0.1% Ag/SA5562 catalyst was used as the base material for all electroless deposition (ED) derived samples. The ED bath used $AgNO_3$ as the source of Ag^+, formaldehyde (HCHO) as the reducing agent (RA), and NH_4OH as needed to maintain pH 11. The $AgNO_3$ solution and HCHO solutions were added from two different motor-driven syringe pumps at a fixed molar ratio of [HCHO]/[Ag^+] = 2/1. The Ag weight loadings deposited by ED were determined by controlling the duration of pumping time of RA (6.0×10^{-2} M) and Ag salt (3.2×10^{-1} at pump speeds of HCHO (11.30 ml/h) and $AgNO_3$ (11.45 ml/h) into an agitated ED bath at pH 11. The bath solution was peristaltically pumped to the base of a vertically- mounted 15 ml tube and the flowrate adjusted until the 842–400 μm (20/40 mesh) particles behaved as a percolating catalyst bed to give good convective mixing of the catalyst particles with the ED components. At the top of the tube, the solution was filtered through a glass frit to remove and maintain the fines in the tubular percolating bed and then recirculated back to the stirred bath as shown in Fig. 6. Initial attempts using a magnetic stirrer bar in the ED vessel resulted in attrition of the catalyst particles to produce fines, which changed diffusion characteristics during catalytic reaction. Control experiments indicated the absence of electrostatically adsorbed Ag on the α-Al_2O_3 support and that there was no thermal reduction of the HCHO and Ag^+ solution. Elemental analyses were made using inductively coupled plasma-optical emission spectroscopy (ICP-OES, Perkin Elmer Avio 200) of periodically collected aliquots of liquid samples. All vessels, tubing, and the pump liner were constructed from inert plastic or Teflon and were cleaned with 37% nitric acid, and thoroughly rinsed with DI water between samples.

Following electroless deposition, all samples were filtered and washed with 1 L/g-catalyst of deionized (DI) H_2O to remove residual ED byproducts and unreacted components. The catalysts were then dried overnight in vacuo at 110 °C and reduced at 200 °C using the same conditions used for the 0.1% Ag/SA5562 base cata-

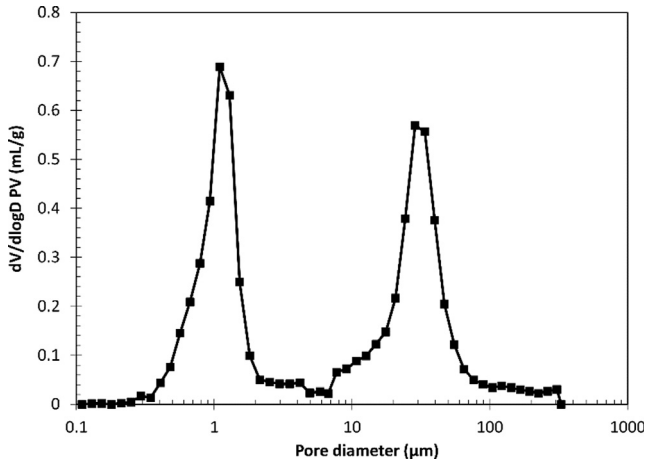

Fig. 3. Pore size distribution for St Gobain SA5562 a-Al_2O_3 determined by Hg intrusion.

lyst. Nominal Ag loadings on α-Al_2O_3 that were determined from analysis of periodic aliquots were confirmed to match results after digestion of the catalyst in concentrated 37% nitric acid and ICP analysis.

2.2. Catalyst characterization

Temperature programed oxidation (TPO) and temperature programed reduction (TPR) experiments were performed using Brooks 5850E mass flow controllers to deliver specific feed compositions to 200 mg samples in a quartz micro-reactor using a high wattage, split-tube furnace (capable of linear heating up to 60 °C/min) connected to an Inficon Transpector 2 Mass Spectrometer using a modified Varian 951 variable leak valve customized for fast detection [24]. Samples were loaded into a ¼-inch quartz tube supported on a quartz plug, dried in-situ at 120 °C for 1 h, then cooled to room temperature in flowing (30 SCCM) Ar. For TPO, 10% O_2 with balance Ar was introduced to the system and samples were ramped at 20 °C/min to 600 °C while monitoring for CO_2 (m/e = 44) and H_2O (m/e = 18). For TPR, samples were heated to 500 °C at 20 °C/min or, alternatively, heated in a separate experiment to 200 °C at 20 °C/min, maintained for 4.5 h, and then ramped to 260 and 340 °C to verify the absence of residual nitrates from $AgNO_3$ decomposition (NO^+ at m/e = 30).

A Micromeritics ASAP 2020 was used for Kr BET analysis, and for chemisorption of exposed Ag sites, H_2 titration of oxygen precovered Ag (Ag—O) was performed using a Micromeritics 2920 pulsed chemisorption analyzer using the method of Vannice [13]. Prior to analysis, samples were heated to 200 °C at 10 °C/min in flowing 10% O_2 with balance He and held for 10 h to remove any potential residue from formaldehyde during ED. After this, the samples were reduced for an additional 2 h at 200 °C in 10% H_2, balance Ar before cooling to 170 °C and purging with flowing Ar. Samples were then exposed to 10% O_2, balance He for 30 min to saturate the Ag surface with Ag—O species before conducting the pulsed H_2 titration, also at 170 °C. Each sample was given two additional sequences of H_2 titration and results are reported as an average; the standard deviation between in-situ titration cycles showed good H_2 uptake agreement for both fresh and used catalysts indicating a stable Ag surface.

Aberration-corrected JEOL 2100F scanning transmission electron microscopy (STEM) was used for Z-contrast imaging with a 200 kV field emission gun and a double tilt holder for tilting the sample across a range of angles (±20°) for obtaining images. Sample preparation involved direct deposit of ground powder on a copper TEM grid with a thin holey carbon coating. Scanning electron microcopy (SEM) was also performed using a Zeiss Gemini 500 equipped with a secondary electron detector (SE2). SEM samples were crushed, applied to carbon backed adhesive tape, and coated with a thin layer of Pd-Au using a Denton Desk II sputter coater with global rotation and tilt. SEM images were collected using an SE2 detector at 5KV beam energy and particle counting was performed with ImageJ software version 1.8.0–172. Great care was taken to ensure that each sample was well represented with >15 images collected at various positions with magnification to give accurate detail at the 200 nm scale.

2.3. Catalyst evaluation

Catalyst evaluations were performed in a parallel flow system consisting of six stainless-steel reactors of 0.25″ OD and 0.035″ wall thickness to give reactor ID = 0.180″ loaded with 3.0 g of 20/40 mesh samples supported on a plug of glass wool. Each reactor tube was press fit into a 1″ OD aluminum sheath to improve isothermal performance. Reactors were heated by 1″ ID × 15″ long BriskHeat heating mantles tightly fitted around the aluminum (Al) jacket. Temperatures were controlled and recorded using a 1/16″ thermocouple embedded in the Al sheath such that the tip was in contact with the outer stainless-steel wall. We have observed that a ¼" OD reactor press fit inside a 1″ OD Al jacket gives essentially an isothermal bed profile with control experiments showing a maximum gradient of 2 °C between the jacket temperature and the center of the catalyst bed which was measured using a sliding thermocouple embedded in a thermowell. The master reaction feed stream consisted of 25% C_2H_4 (Praxair, EY 2.5-T), 8% O_2 (Praxair, OX 4.3UH-T), balance CH_4 (Praxair, ME3.7UH-T) and was blended using Brooks 5850E mass flow controllers. No ethyl chloride (EtCl) modifier was added to the feeds in this series of experiments to avoid potential issues that might arise from unequal rates and extents of Cl addition for different particle sizes and masses of Ag [25]. The master feed composition was plumbed to a second manifold of mass flow controllers which provided 50 SCCM (GHSV 1000 hr^{-1}) to each reactor at a pressure of 250 psig. Reaction pressures were let down to 1 atmosphere pressure using Parker Veriflo ABP1 series back pressure regulators maintained at 120 °C. All other product streams were also heated to 120 °C to avoid condensation and were sampled automatically using a six-stream Valco sample valve at 2-hour intervals using an Agilent 7890A gas chromatograph (GC) equipped with two Poraplot-Q columns (30 m × 0.32 ID, 19091P-QO4) connected to a TCD for CO_2, EO, and H_2O analyses and a separate FID for trace amounts of ethylene glycol and acetaldehyde (never observed). Carbon mass balance calculations between the feed and the product streams for CO_2, EO, and C_2H_4 gave carbon balances of 100 ± 0.5%. All reaction order studies were performed at <10% C_2H_4 conversion and Weisz-Prater calculations indicated the absence of internal mass transfer limitation at maximum EO formation (W-P = 5.5 × 10^{-4} at 3.2 mol% EO, 12 wt% Ag/SA5562).

EO isomerization studies were performed in the same reactor system used for catalyst evaluation, except a 2.1% EO balance He mixture (AirGas) was blended with O_2 and CH_4 to give feed concentrations of 0.5 %EO, 8% O_2, and balance He + CH_4; 100 SCCM of mixed gas was supplied to each reactor containing 2.0 g of sample at atmospheric pressure. One reactor was left empty to determine thermal, empty tube EO conversion and mass balance of the isomerization reaction; isomerization measurements were conducted at 220, 245, and 270 °C.

3. Results and discussion

3.1. Isomerization study

Fig. 4 illustrates the effect of temperature on the isomerization of EO for α-Al_2O_3 (SA5562) and 12 wt% Ag/SA5562. At 245 and 270 °C, EO conversions for SA5562 were 5.1%/m^2 and 13.5%/m^2, respectively, with acetaldehyde (HAc) being the only product detected; the amount of isomerization approached 0% conversion at 210 °C, the temperature used for catalyst evaluation. Thus, we can ignore the consecutive support-catalyzed isomerization of EO in our Ag size effect evaluations. Interestingly, both EO and HAc were thermally stable even at 270 °C. Neither epoxide ring opening of EO or scission of one of the three reactive α-C-H bonds of HAc occurred, indicating the thermal oxidative stability of both oxygenates at high temperatures. Note that when an amount of Li^+ corresponding to 0.5 ML (assuming 1.2×10^{19} sites/m^2 surface) was added to neutralize residual acid sites on α-Al_2O_3, acidity was reduced even further to give a largely isomerization-free catalyst support. However, at similar conditions for 12 wt% Ag/α-Al_2O_3, considerably more EO underwent combustion to form CO_2 and H_2O, indicating that consecutive combustion had occurred on Ag sites. At 245 °C, EO conversion had increased from 5.1% to 20.0% when 12% Ag was present. This does not mean that combustion levels of EO this high occur at typical reaction conditions for promoted catalysts, where, in addition to a large number of inorganic promoters [22,26,27] and the presence of ppm levels of ethyl chloride (EtCl) in the gas feed [28,29], there are other gas phase components adsorbed more strongly on the Ag surface. Reported reaction orders [30,31] for EO formation over Ag catalysts are near zero order for C_2H_4, negative partial reaction orders for CO_2, and near first order for O_2. Thus, the Ag surface is Ag-O limited at typical reaction conditions which would necessarily inhibit EO combustion.

3.2. Electroless deposition

Water-soluble $AgNO_3$ was selected as the Ag source for base catalysts synthesis of 0.1% Ag/SA5562 due to its clean thermal decomposition as shown in Fig. 5. Temperature programed reduction (TPR) was performed on a portion of the 12 wt% Ag/SA5562 sample where the catalyst precursor was heated at 20 °C/min in flowing 10% H_2, balance Ar up to 200 °C and NO was monitored at m/e = 30; there was a sharp and symmetrical peak centered at ~240 °C with a small shoulder at ~340 °C. To determine whether reduction would occur at 200 °C by maintaining that temperature for a longer period of time, the plot in Fig. 5 (right) was obtained, indicating that complete reduction occurs within a time period of 120 min. No additional NO peak was observed at higher temperatures. The TPR experiments confirmed that reduction at 200 °C was sufficient for reduction, helping to minimize thermally driven Ag particle sintering.

The electroless deposition (ED) bath was developed from prior work for the deposition of Ag [20,32] on Pt and Pd base catalysts. Formaldehyde was selected as the reducing agent based on results of Djokic [33] and Ohno [34] for ED on Ag surfaces. Control experiments for thermal instability indicated that reduction of $AgNO_3$ was kinetically slow. Following a period of 128 min where $AgNO_3$ and RA were syringe pumped into a beaker containing only DI water, only 5% of the Ag^+ in solution was reduced to Ag° and that occurred at rather high concentrations of 0.81 umol Ag^+/ml and 102 umol-RA/ml; these data are shown in Fig. 7. In the presence of a Ag catalyst, the rate of electroless deposition greatly exceeds the rate of thermal instability so the concentrations of Ag^+ and HCHO never reach critical concentrations for thermal reduction

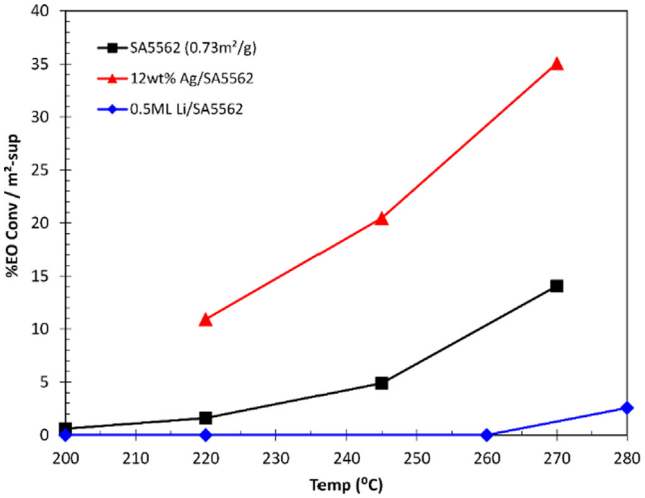

Fig. 4. EO isomerization activity as a function of reactor temperature (Feed Composition: 0.5% EO, 8 %O_2, Bal CH_4, 14.7 psig, GHSV 2700 h^{-1}). Acetaldehyde was the sole product detected at 270 °C for Ag free SA5562 α-Al_2O_3. With the addition of 12 wt% Ag, EO conversion increased and only combustion products were observed. For the 12 %Ag/SA5562 sample, data were not collected at 200 °C.

to occur [35]. Theoretical Ag weight loadings were confirmed by digestion and ICP analysis of the ED samples following ex-situ reduction in flowing H_2 further, indicating that none of the reduced Ag existed as nanoparticles in solution.

Initial ED experiments were performed using a continuous ED bath where catalysts, RA, and salt were added to a beaker and agitated using a stir bar [20]. With this configuration, only 40% of the 20/40 mesh material was recovered; the remaining 60% was ground to fine powder. Consequently, a percolating ED bed shown in Fig. 6 was developed where RA and $AgNO_3$ solutions were syringe pumped into an agitated reservoir containing DI water. A peristaltic pump transferred the ED solution at a rate sufficient to cause percolation and thorough mixing of the catalyst and ED components. Catalyst particles and any fines were maintained in the percolation bed using a glass frit exiting at the top of the tube. Mass recovery of the 20–40 mesh material approached 100% for all samples used in this study.

Fig. 7 displays the rate of deposition for all catalysts prepared in this study. All higher weight loading samples derived from the common 0.1 wt% Ag base catalyst have similar rates of Ag deposition indicating good reproducibility and the absence of experimental artifacts. The sluggish reduction of Ag^+ over the initial 60 min can be attributed to the kinetics of deposition. Previous work demonstrated Ag ED on Pt to be first order in Pt sites with a high factional order in HCHO, and zero order in Ag^+ concentration [32], indicating that HCHO activation on Pt was the kinetically slow step. Where Pt is an effective catalyst for hydrogen abstraction [36], Ag is relatively weak and requires higher HCHO concentrations before electroless deposition becomes favorable. The percolating ED bath demonstrates an effective strategy for controlling particle size with only a minor modification to the ED configurations previously published [20,32,35,36] and can be adapted to synthesize catalysts on a variety of formed supports potentially suitable for industrial applications.

3.3. Characterization

Catalyst characterization focused on the determination of size and distribution of Ag particles using gas adsorption and microscopy techniques. X-ray diffraction was not performed because particle sizes exceeded the diameters required for accurately using

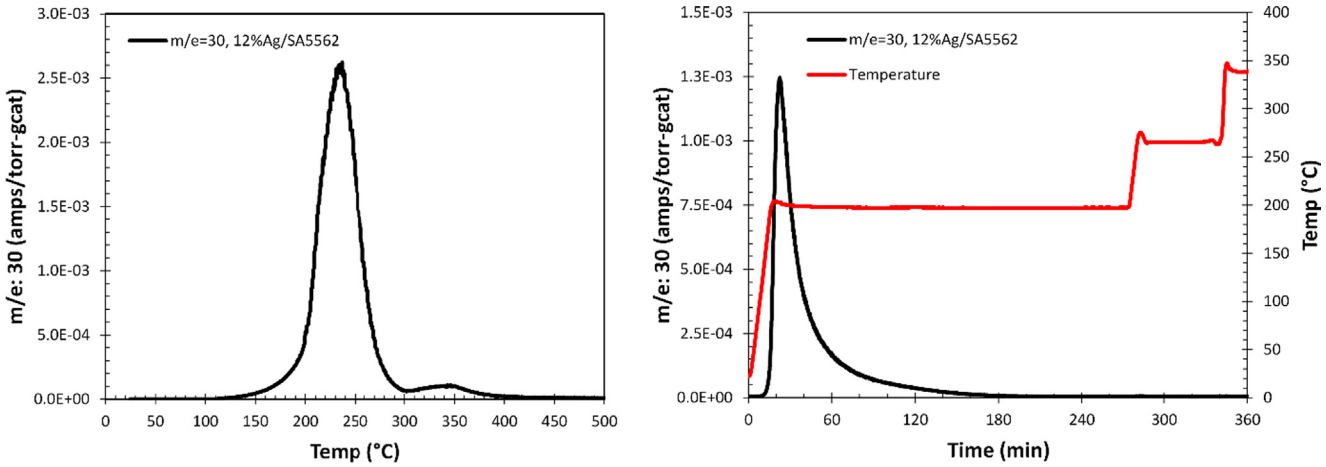

Fig. 5. Nitrate decomposition by reduction of 12 %Ag/SA5562 in 20 sccm of flowing 10% H_2 balance Ar. Experiment 1: The sample was heated from 25 to 500 °C at 20 °C/min (Left). Experiment 2: The sample was held at 200 °C for 4hrs then ramped to 265 and 340 °C to check for residual nitrate compounds (Right).

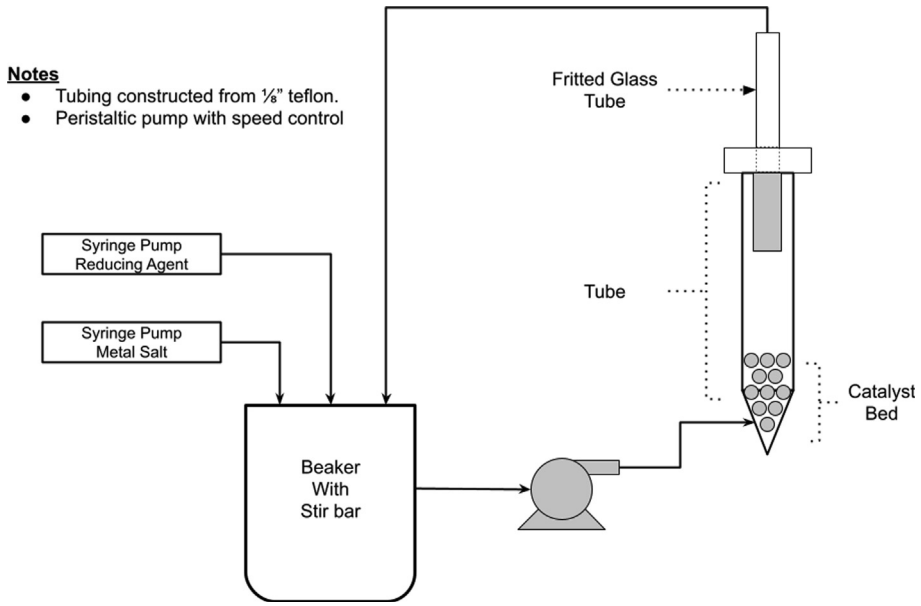

Fig. 6. Configuration for a percolating bed electroless deposition bath with continuous recycle.

FWHM values and the Scherrer equation. Chemisorption using H_2 titration of O-precovered Ag was used to determine the concentration of Ag surface sites to calculate average Ag particle sizes assuming either spherical or hemispherical geometries. More importantly, it determines the actual number of surface Ag sites for calculation of turnover numbers to test for structure sensitivity of EO formation. Typical examples of H_2 uptake plots are shown in Fig. 8 for 0.1 and 12.0 wt% Ag. Note the significant uptake for Ag loadings as low as 0.1 wt% (requires 4.0 g of sample) demonstrating the sensitivity of a 1:1 H_2 to Ag-O titration stoichiometry.

A summary of particle sizes determined by H_2 titration and SEM are displayed in Table 2. Results for fresh samples prepared by electroless deposition and reduced in flowing 20% H_2 balance Ar at 200 °C for 4 h indicate particle sizes are larger for higher levels of Ag^+ deposition. The 12 wt% Ag sample prepared by incipient wetness of $Ag_2C_2O_4$ shows a significantly different average particle size likely related to the oxalate complex [37] or the ethylenediamine (EN) ligand which may help anchor Ag^+ to the rather featureless α-Al_2O_3 surface [38]. In fact, TPD experiments showed residual EN was stable on the Ag/α-Al_2O_3 surface up to 250–260 °C, so stabilization is certainly possible.

SEM particle diameters were measured at the longest particle dimension (for non-spherical geometries) using 400–1000 crystallites and are reported in Table 2 as the surface average diameter $D_s=\sum n_i d_i 3/\sum n_i d_i^2$, where n_i is the number of particles with diameter d using a 10 nm bin spacing and hemispherical geometry [39]. Particle size determinations were also made using the particle size corresponding to the highest concentration of Ag surface sites. This was calculated using the particle size distribution determined by SEM and applying it to the full Ag weight loading; key parameters for this method include the Ag atom volume in a low index plane (17.1 $Å^3$) and a projected surface area of 8.7 $Å^2$ for these Ag atoms [9]. This formalism is displayed in Fig. 10 where histograms based on the number of particles measured are shown as black bars overlayed with a red line plot denoting the number of Ag surface sites for that bin size. The samples containing 0.1 and 0.3 wt% Ag have

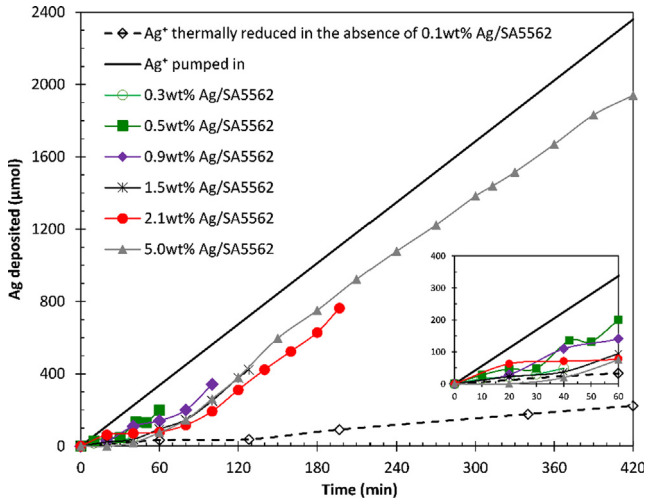

Fig. 7. Thermal stability of ED bath and kinetic deposition profiles for samples made in this study. No thermal instability was detected before 120 min. All ED samples were prepared using a common 0.1 wt% Ag/SA5562 base catalyst. Bath conditions: pH 11, HCHO /$AgNO_3$ (2/1), 30 °C. Ag concentrations were determined by ICP analysis.

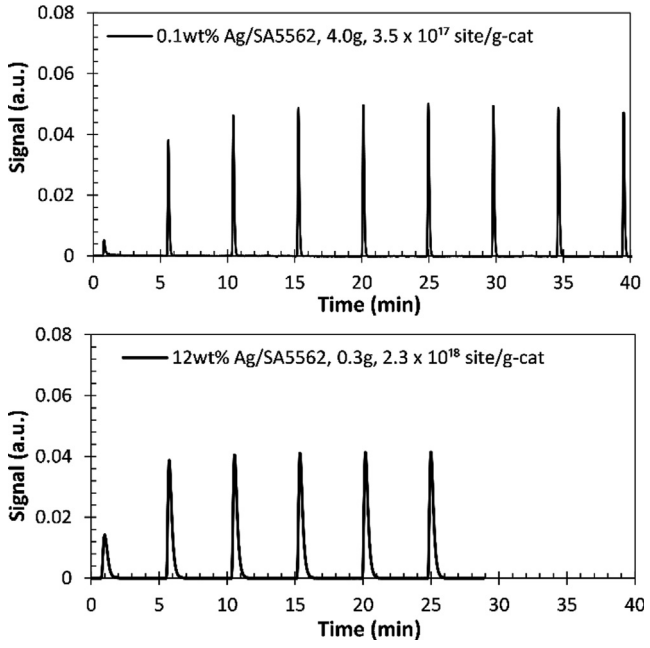

Fig. 8. Pulsed H_2 uptake for the hydrogen titration of oxygen precovered Ag at 170 °C for fresh samples of 4.0 g of 0.1% Ag/SA5562 (top) and 0.3 g of 12% Ag/SA5562 (bottom).

relatively narrow distributions and the particle sizes based on the number of Ag surface sites agree quite well with particle counts; as the distribution of Ag particle sizes broaden the deviation between the two different SEM methods begins to diverge and indicate those particles with the highest number of active sites are larger than the surface average diameter.

SEM-derived particle sizes were also in general agreement with those calculated from H_2 titration for Ag loadings on fresh samples between 0.3 and 5.0 wt%. The difference in particle sizes comparing chemisorption and SEM for the 0.1 wt% Ag sample in Table 2 is likely due to the presence of ultra-small nanoparticles below the limit of detection by SEM but visible by high magnification STEM (Fig. 9) that also show activity for H_2 titration. In Fig. 10, there is additional evidence for the existence of small particles for the 0.1 wt% Ag sample following epoxidation at 210 °C; small Ag clusters apparently sintered to form larger particles that are visible using SEM. A similar trend is observed for the 0.5 wt% (Fig. 10) sample where a higher density of particles appears after Ag^+ deposition on previously non-visible Ag sites.

Particle size measurements using H_2 titration following reaction indicated growth for all samples, but most notably for the 0.1 wt% Ag sample; the fresh sample corresponded to 19 nm Ag particles compared to 240 nm for the spent sample (Table 2). However, SEM analysis showed an apparent growth from 44 to only 67 nm in diameter. Temperature programmed burnoff (TPO) curves in Fig. 11 for the spent 0.1% Ag sample suggest the presence of extensive carbon fouling; the partially-resolved peaks centered at 225 and 370 °C are attributed to carbon-based foulant in contact with both Ag and alumina surfaces, respectively. STEM analysis of the spent 0.1 wt% Ag sample also showed the appearance of fluffy, carbon deposits on the spent material and suggest the burnoff peak at 370 °C is associated with carbon at the perimeter of the Ag-alumina interface and represents both thermal and Ag-catalyzed burnoff. In the interior of the carbon fluff, some small Ag particles appear to be encapsulated by the carbon deposits. The broad peak centered at 350 °C for the fresh sample suggests some residual hydrocarbon residue remained from preparation of the base 0.1 wt% Ag sample.

A foulant factor (λ) denoting the extent of Ag fouling can be calculated according to Eq. (1) where the decrease in number of hydrogen titration sites is reduced by surface foulant (first term), which must be adjusted by the number of exposed Ag sites lost from particle sintering that occurred during reaction. Terms C_f and C_s denote the number of Ag sites determined by H_2 titration for the fresh and spent samples, respectively, and the second term corrects for particle sintering during reaction; S_f and S_s denote the concentrations of Ag surface sites determined by SEM before and after reaction, respectively.

$$\lambda = \left(\frac{C_f}{C_s}\right)\left(\frac{S_s}{S_f}\right) \quad (1)$$

Foulant factors equal to unity represent samples that exhibit no sintering and no fouling during reaction. Values >1 indicate fouling has occurred and for <1, some Ag particles have undergone redispersion and that fouling is non-existent. The results in Fig. 12 imply that samples composed of particles below 100 nm in diameter are more likely to accumulate carbon deposition and to sinter as indicated by λ values of 8.1 and 2.5 for the 0.1 and 0.3 wt% samples respectively. Histograms for the spent 2.1 and 5.0 wt% samples in Supplemental Fig. S2 suggest a possible re-dispersion of particles above 200 nm with some Ag particles observed between 50 and 75 nm following reaction. Hensen [40] noted a similar behavior for 5 and 10 wt% Ag/α-Al_2O_3 catalysts prepared by incipient.

wetness of $Ag_2C_2O_4$ for particles >100 nm when vinyl chloride was included in the feed. Even if higher Ag loadings catalysts contain some Ag particles <50 nm, these particles make little contribution to the total number of accessible sites. The results in Table 2 confirm that Ag particles smaller than ~80 nm sinter quite readily, particles between 100 and 200 nm appear to be stable, and particles >300 nm seem to show some measure of particle redispersion.

3.4. Evaluation

Ethylene epoxidation rates were measured at 210 °C using a feed of 25% C_2H_4, 8% O_2, and balance CH_4. As stated earlier, ppm levels of ethyl chloride feed additive were omitted to avoid potentially different rates of Cl deposition on different sized Ag particles

Table 2
Catalysts prepared by ED of Ag on 0.1 wt% Ag/SA5562.

Catalyst	Fresh samples			After reaction		
	Chemi (nm)	SEM[A] (nm)	Active site max[B] (nm)	Chemi (nm)	SEM[A] (nm)	Active site max[B] (nm)
0.1Ag/SA5562	19	44 ± 12	20	240	67 ± 19	40
0.3Ag/SA5562	80	84 ± 30	90	294	112 ± 37	90
0.5Ag/SA5562	85	90 ± 26	90	119	92 ± 27	70
0.9Ag/SA5562	148	160 ± 54	150	182	172 ± 63	180
1.5Ag/SA5562	201	138 ± 46	120	238	157 ± 47	150
2.1Ag/SA5562	220	211 ± 67	190	290	212 ± 71	210
5.0Ag/SA5562	292	381 ± 154	370	520	300 ± 112	280
12Ag($Ag_2C_2O_4$)/SA5562	284	172 ± 60	140	463	160 ± 54	160

[A] Results generated from 400 to 1000 particle measurements. Details in Supplemental Fig. S2.
[B] Particle size shown represents that which contains the maximum number of active sites within the SEM particle size distribution.

[40]. Turn over frequencies (TOF) are reported at steady state reaction conditions, typically after approximately 65 h on-line, although some samples took longer to achieve steady state. A representative time on stream (TOS) plot for the 1.5 wt% Ag sample is displayed in Fig. 13 for a reaction period of 300 hrs. Gaps in the data are periods where EO work rates, defined as mole % EO in the product stream at standard conditions of flow rate and temperature, were varied to determine intrinsic selectivity (Fig. 16) or represent the initial 20-hour startup where catalyst performance is quite transient.

Similarly, the other catalysts were evaluated and the data used to generate TOF plots shown in Fig. 14 and summarized in Table 3. The concentrations of active sites required to calculate TOF values are based on H_2 titration values of the spent catalysts, since they best represent the state of the catalyst when steady state rates are reached; further, H_2 titration is a direct measurement that effectively "counts" the number of active Ag sites and does not assign a value based on a specific method of particle size measurement and distribution. Interestingly the TOF = 0.12 s^{-1} for 12 wt% Ag/SA5562, denoted as an open black triangle in Fig. 14, with an active site concentration of 1.66 × 10^{18} Ag/g cat agrees within a factor of 2× for all the ED-derived samples. With the exception of 0.1 and 0.3Ag/SA5562 there were no significant particle size effects between the diverse range of particle sizes and geometries of a "conventional" catalyst compared to those of this study.

The relatively high TOF values of 0.24 and 0.34 s^{-1} for the 0.1% and 0.3% Ag samples, respectively, are very likely artifacts of the low concentrations of Ag sites measured by H_2 titration (Table 3). The values that were measured by chemisorption were at the lower level of sensitivity of the instrument. The combination of fouling and sintering of small Ag particles during evaluation makes it very difficult to quantify any possibility of structure sensitivity for Ag particles <50–70 nm in diameter. Regardless, for calculation of TOF values, the number of active sites should be directly measured, as in chemisorption, and not inferred from measurement of a limited number of particles, and preferably after reaction, when steady state has been reached. The results in Fig. 14 show that as Ag particle diameters increase from 90 to 300 nm, the TOF values for EO formation increase only from 0.08 to 0.18 s^{-1} before reaching an asymptotic maximum. The similar TOF value of 0.12 s^{-1} for the 12 wt% Ag/SA5562 sample shown in Fig. 1 with a wide range of Ag particle sizes and morphologies confirms the negligible structure sensitivity of Ag for ethylene epoxidation. Van Hoof [19] also noted that TOF values for C_2H_4 oxidation varied only by a factor of <2 over the Ag particle size range from 50 to 170 nm at similar reaction conditions; Ag surface site concentrations were determined from TPD of O_2 from an O_2-pretreated catalyst surface before reaction. Our results also agree with earlier work of Wu [41] who found that activities for ethylene conversion were very low for particles <5 nm. Harriott [42] reported that Ag particles <3 nm were inactive for EO formation, although the very low activities made it difficult to determine selectivity with accuracy. Goncharova [43] studied Ag catalysts with sizes ranging from 10 to 100 nm in size and observed that ethylene epoxidation increased 20-fold as Ag particle sizes increased from 30 to 50 nm in size. However, results were obtained using a recirculation loop reactor operated at one atmosphere pressure and a feed of 2% C_2H_4 and 7% O_2; the reactor and reaction conditions were very different from those used at normal conditions. Thus, it is difficult to place their results in perspective.

Verykios [15] evaluated four different families of Ag catalysts supported on different, low surface area aluminas and found the TOF for EO increased as Ag particle sizes increased from ~50 to 200 nm in size and postulated that changes in surface morphology likely accounted for these changes. However, the statistical models of Van Hardeveld and Hartog [44] for fcc metals such as Ag indicate that after particle sizes reach 50 nm in diameter they have essentially a constant surface composition of approximately 75–80% (111), 15–20% (100), and balance of (100)–(111) and (111)–(111) edge sites; corner sites are negligible. Boudart also argued that structure sensitivity due to different types of surface sites are valid only between 1 and 5 nm in size [45]. If structure sensitivity exists for larger particles, it is due to other reasons.

Finally, in more recent work de Jongh and co-workers [18] evaluated a series of Ag catalysts supported on α-Al_2O_3 with particle sizes ranging from 28 to 500 nm and found that while 28 nm particles had a very low TOF value, the next larger particle size of 62 nm had reached the maximum TOF of 6 s^{-1} which was essentially maintained up to 500 nm Ag. Silver particle sizes were determined by SEM analysis of fresh samples. TOF values of 6 s^{-1} are quite high for olefin epoxidation; values are typically in the range of 0.5 s^{-1} [46]. More importantly, an alternate explanation for the low activity of the 30 nm particles was that the particles were covered by organic foulant, as observed in the present study. In earlier work for epoxidation of 1,3-butadiene, Monnier [46] also observed that the strongly adsorbed precursor for the selective epoxidation product, 3,4-epoxy-1-butene (EpB), resulted in virtually complete loss of activity after 24 hr and limited EpB selectivity to 50%. When ppm levels of Cs were added to the Ag catalyst, desorption of EpB was facilitated; activity increased by >30×, catalyst lifetimes improved from hours to months, and selectivity was improved from 50% to 95% with balance of only CO_2/H_2O.

A key question then is why small Ag particles exhibit carbonaceous fouling. Schlögl et al. [47,48] used XANES and NA-XPS (in-situ XPS at mbar O_2 and C_2H_4 pressures) and proton-transfer reaction mass spectrometry to determine the amounts of nucleophilic (non-selective) and electrophilic (selective to EO) oxygen species on Ag surfaces. They concluded that nucleophilic oxygen leads not only to non-selectivity to EO but also fouling and subsequent deactivation of the Ag surface, presumably by the higher binding energy of O to the Ag surface which makes desorption of EO or its precursor from the Ag surface more difficult. They suggested

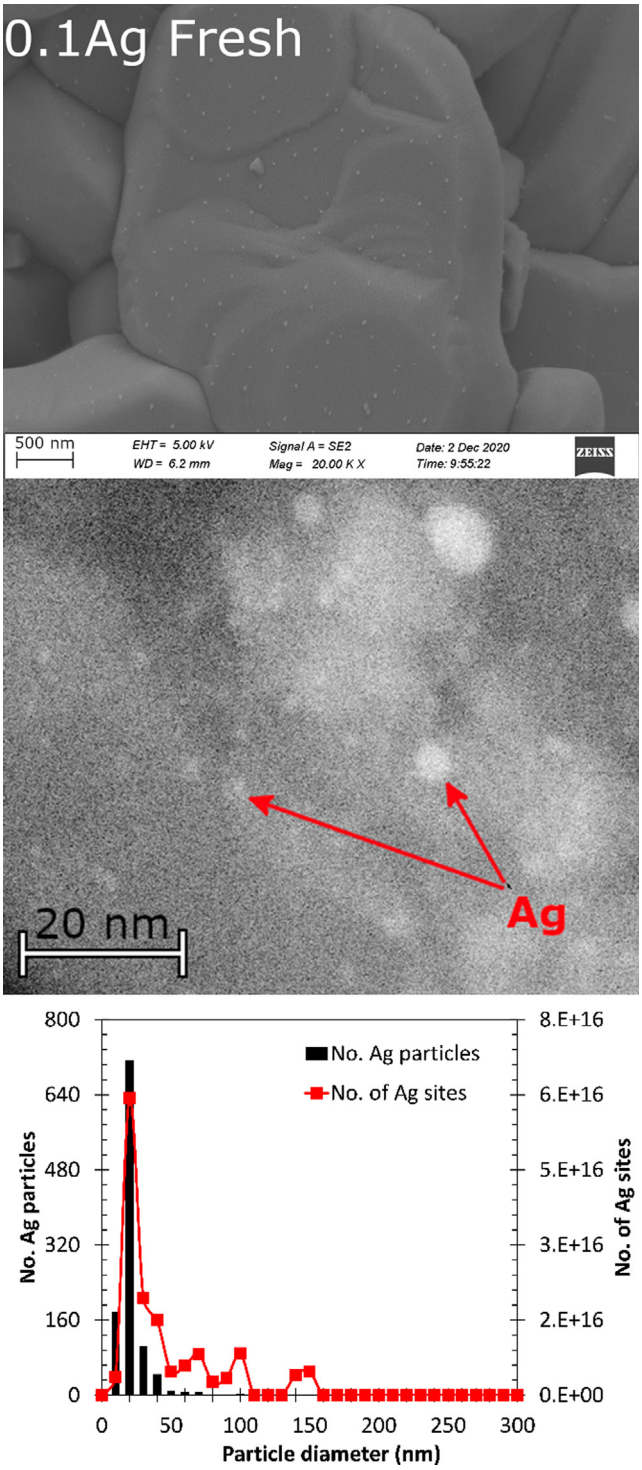

Fig. 9. SEM (top), STEM (middle), and histogram (bottom) from fresh 0.1Ag/SA5562 following reduction at 200 °C.

that the nucleophilic oxygen they measured is best described as a surface oxide owing to the similarity between its O K-edge spectrum and that of the bulk oxide Ag_2O, related to the oxidized surface of small Ag particles. Waugh [49] also concluded that EO selectivity is a function of the Ag—O bond strength; the weaker the Ag—O bond is, the more selective it is. The.

Ag—O—CH2—CH2 intermediate formed on a Ag surface having the stronger Ag—O bond, such as a stepped surface or on a small Ag particle, will have a greater probability of being involved in unselective H abstraction reactions by the more electronegative surface O atoms than cyclising to form EO. If the strongly bound intermediate is unable to abstract the strongly bound O, then fouling will result, and activity permanently lost.

We have also conducted power rate law kinetic analyses for ethylene and oxygen dependencies for these catalysts to determine if the kinetic dependencies are different for the different samples, which would imply a change in the rate determining step(s) of epoxidation. The results in Fig. 15 show the reaction orders for O_2 were essentially constant at 0.8–1.0 and for C_2H_4 between 0 and −0.2 for samples with Ag particle sizes between 67 and 212 nm (SEM analysis, after reaction). These reaction orders are similar to those determined by many others for EO formation at relatively typical reaction conditions [30,50–53] showing there is no change in the rate determining step(s) and that the mechanism is independent of particle size.

Selectivities for EO formation show a greater dependency on Ag particle sizes. In Fig. 16 selectivities to EO are plotted as functions of EO concentrations. The y-intercept is the EO selectivity at 0.0% EO concentration, which represents the intrinsic selectivity of the Ag surface since there is no gas phase EO which could undergo isomerization to acetaldehyde and then combustion on Ag. The selectivity losses at 0.0% EO formation represent the sum of direct combustion of C_2H_4 or a strongly adsorbed EO intermediate that undergoes combustion before it can desorb as EO. The results in Fig. 16 show two major groupings of EO selectivity vs. EO concentration plots. For Ag particles <100 nm, the intrinsic EO selectivity is ~60%, while for Ag particles >150 nm, the value is ~75%. Thus, the selectivity trends track well with fouling characteristics and, by extension, the transition from strongly-bound, nucleophilic Ag—O to more loosely-bound, electrophilic Ag—O surface species. This finding is not unlike that observed for butadiene epoxidation [46] where the identity of the foulant, detected by adding trace amounts of epoxybutene (EpB) into the feed, originated from strongly-adsorbed epoxybutene (EpB) precursor intermediates on unpromoted Ag surfaces. With the addition of Cs, selectivity to EpB and C_4H_6 conversion increased from 45% to 92% EpB and 0.8% to 13% C_4H_6 respectively; a finding that is consistent with literature indicating Cs decreases the adsorption strength of the epoxide intermediate [6,7,22,46].

The slopes of the plots in Fig. 16, which are indicative of sequential EO combustion on Ag sites for the 2.1, 5.0, and 12 wt% Ag samples are very similar, suggesting there are no particle size effects between 157 and 300 nm Ag particles for Ag-catalyzed combustion of reabsorbed EO.

This manuscript has focused on Ag particles size to improve TOF and selectivity; however, working catalysts use a variety of different-functioning promoters to adjust catalyst performance. These effects are much greater than Ag particle size-linked characteristics as shown in Fig. 17 where EO selectivity is plotted as a function of catalyst work rate for an unpromoted 12 wt% Ag/SA5562 and a fully promoted 12 wt% Ag/SA5562 containing promoters, co-promoters, and ethyl chloride co-feed. Samples were evaluated in a typical industrial feed composition containing 25% C_2H_4, 8 %O_2, 2 ppm ethyl chloride (EtCl), balance CH_4 at 250 psig operation. Space time yields for these plots were adjusted by varying gas hourly space velocity between 4,200 and 13,800 h^{-1}. Suppression of sequential EO combustion is demonstrated by the slopes of the line, with the fully promoted catalyst having a value of −1.29 and the unpromoted sample with a value of −5.05. For operation at 2.0 mol% EO in the product stream, these slopes translate to working selectivities of 75% and 90% for the unpromoted and promoted samples, respectively. Note that the samples also have significantly different intrinsic selectivity values, increasing from 85% for unpromoted Ag/SA5562 to 92% for the fully promoted sample. The promoters lower the rate(s) of parallel combustion of

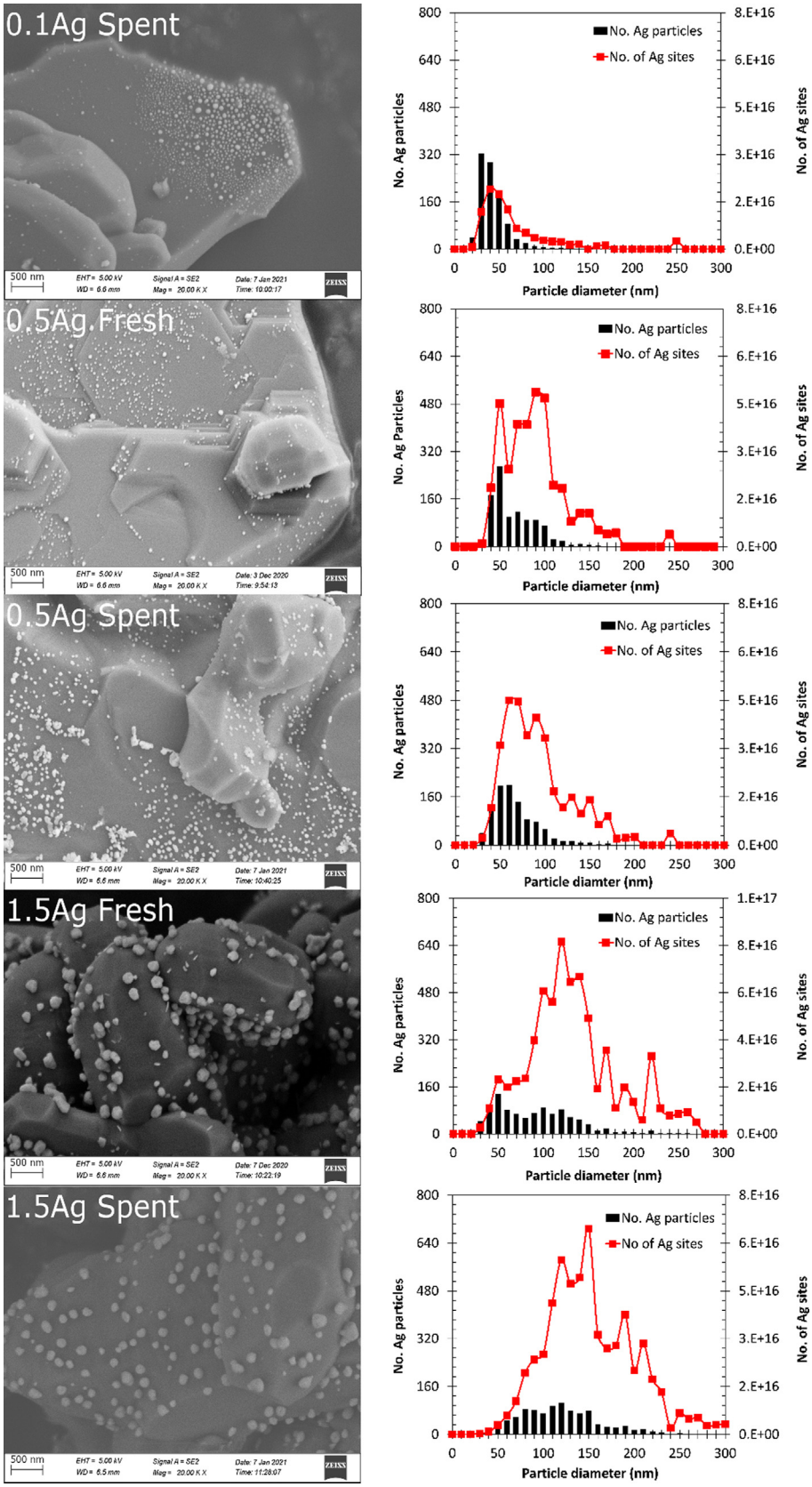

Fig. 10. SEM images for "Fresh" samples treated in flowing 50% H_2 balance He at 200 °C and "Spent" samples after reaction conditions at 210 °C for 200 + h.

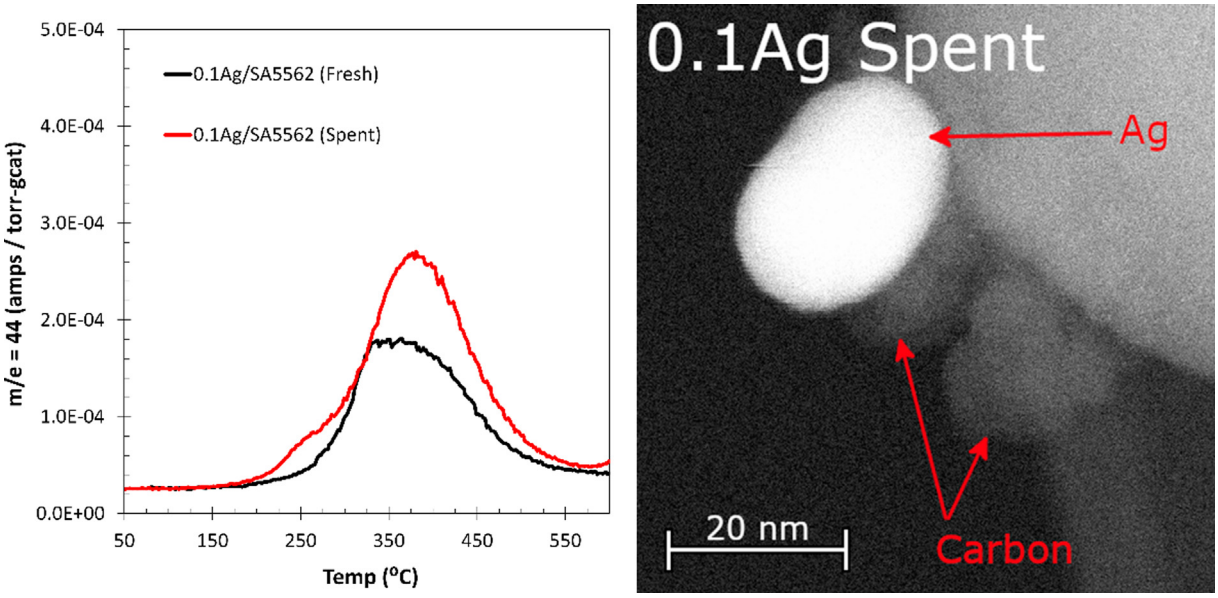

Fig. 11. Temperature programed oxidation of fresh and spent 0.1 wt% Ag catalyst prepared from $AgNO_3$ and SA5562 α-Al_2O_3 (left). STEM image for 0.1 wt% Ag/SA5562 indicating the deposition of carbon following reaction. All experiments were performed with a ramp rate of 20 °C/min and a gas flow rate of 20 SCCM.

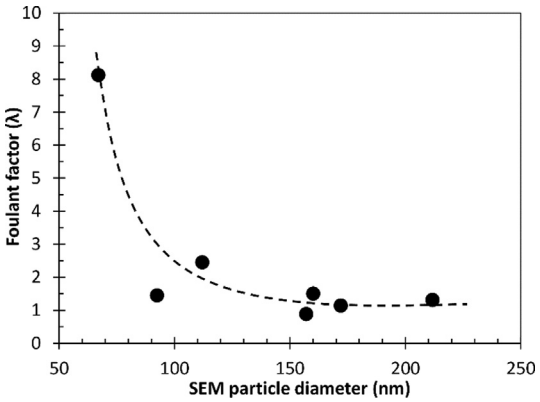

Fig. 12. Foulant factors calculated from fresh and spent H_2 titration result as a function of Ag particle sizes determine by SEM measurements for used samples.

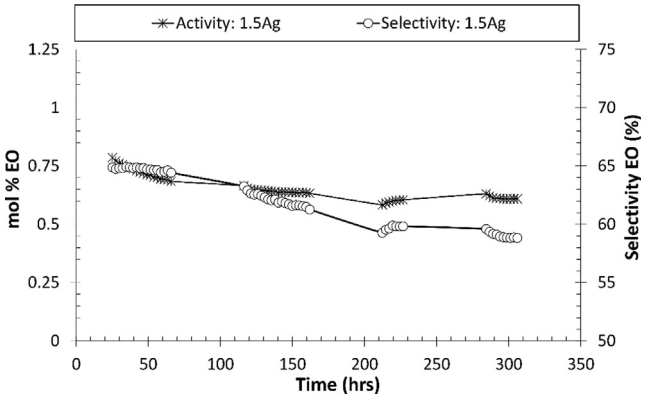

Fig. 13. *Activity and selectivity results for 1.5 wt%Ag/SA5562. Reaction conditions 25% C_2H_4, 8 %O_2, balance CH_4, 210°C,* GHSV 1000 hr^{-1}.

ethylene and/or combustion of strongly adsorbed EO precursors [22,54–58]. These final data in Fig. 17 are included to simply indicate that the use of promoters has been a more fruitful strategy for

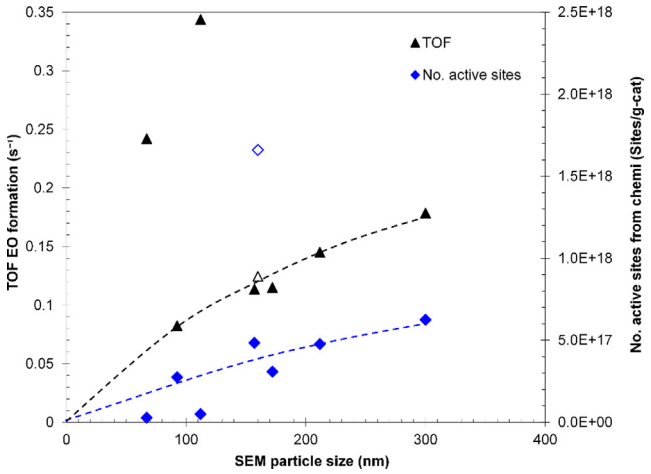

Fig. 14. Turn over frequency for EO formation. Surface area average particle sizes determined from SEM images of samples following reaction. Active site quantities determined from H_2 titration of spent samples. Open markers denote the 12 wt% Ag catalyst prepared from Ag oxalate. Reaction conditions 25% C_2H_4, 8 %O_2, balance CH_4, 210 °C, GHSV 1000 h^{-1}.

obtaining catalysts that are both highly active and highly selective under commercially relevant conditions compared to controlling Ag particle sizes.

4. Conclusions

The use of controlled electroless deposition of different amounts of Ag on pre-existing 0.1 wt% Ag/α-Al_2O_3 was used to prepare a series of supported Ag catalysts with particle sizes ranging from approximately 20–400 nm in diameter. Particle sizes were determined by SEM and selective chemisorption (H_2 titration of O-precovered Ag) both before and after evaluation for C_2H_4 epoxidation at typical industrial reaction conditions. Evaluation showed that only a modest structure sensitivity for ethylene oxide formation exists for supported Ag catalysts. Over the range of 90–300 nm Ag particle diameters, TOF values increase from 0.08 to 0.18 s^{-1}, an

Table 3
Summary of turnover number for EO formation calculated from the quantity of active sites from H_2 titration and particle size distributions from SEM.

Catalyst	TOF, fresh samples (s^{-1})		TOF, spent samples (s^{-1})		Sites from spent chemi (sites/g-cat)
	SEM	Chemi	SEM	Chemi	
0.1Ag/SA5562	0.05	0.02	0.07	0.24	2.82×10^{16}
0.3Ag/SA5562	0.07	0.11	0.10	0.34	5.06×10^{16}
0.5Ag/SA5562	0.06	0.06	0.06	0.08	2.75×10^{17}
0.9Ag/SA5562	0.10	0.09	0.10	0.11	3.09×10^{17}
1.5Ag/SA5562	0.08	0.11	0.09	0.11	4.84×10^{17}
2.1Ag/SA5562	0.11	0.11	0.11	0.15	4.77×10^{17}
5.0Ag/SA5562	0.13	0.10	0.10	0.18	6.25×10^{17}
12Ag($Ag_2C_2O_4$)/SA5562	0.05	0.09	0.04	0.12	1.66×10^{18}

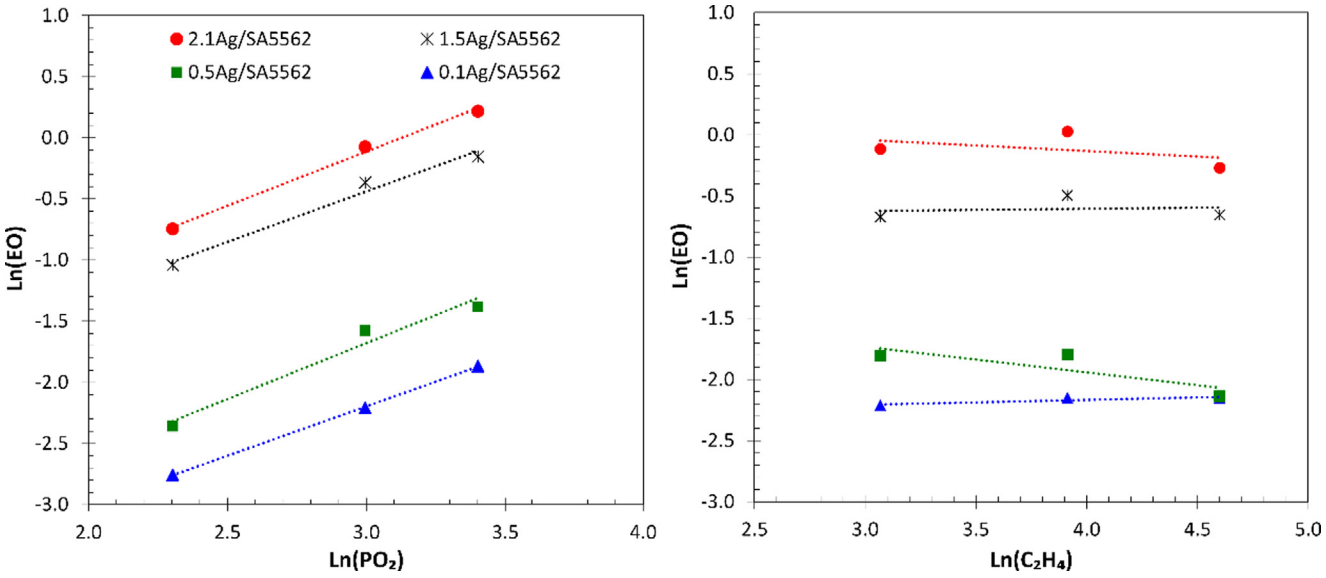

Fig. 15. Oxygen (left) and ethylene (right) reaction orders for catalysts representing Ag particles between 19 and 211 nm in size. Oxygen reaction orders were measured at constant 25% ethylene concentration and ethylene reaction orders were measured at constant 8% oxygen concentration.

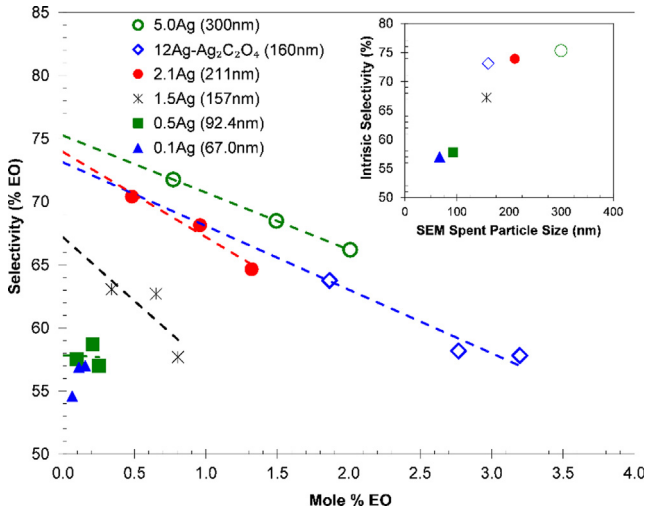

Fig. 16. Activity-Selectivity plot for select samples. The slopes for samples containing >1.5 wt%Ag are in agreement suggesting similar levels of consecutive combustion. Data was collected at 210 °C where EO isomerization on the support was negligible. Feed contains 25% C_2H_4, 8–16% O_2, balance CH_4, GHSV 1000 h^{-1}. No EtCl was added to the feedstream.

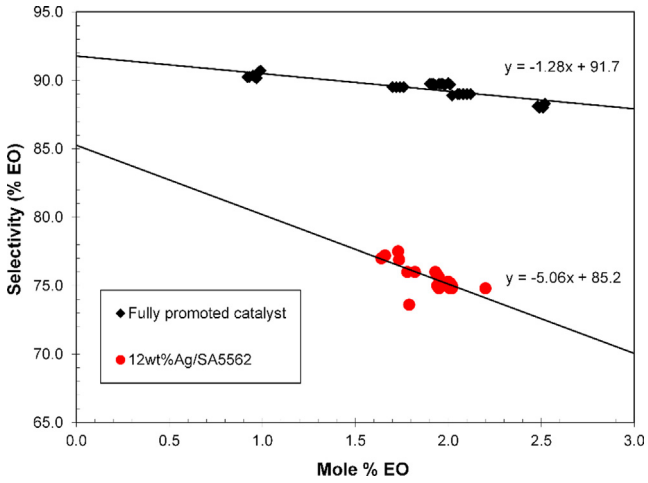

Fig. 17. EO formation vs selectivity to EO for unpromoted 12 wt%Ag/SA5562 and the same fully promoted catalyst. Samples were evaluated in ¼" OD reactors in feed of 25% C_2H_4, 8% O_2, 2 ppm EtCl, balance CH_4, GHSV 4200 h^{-1}.

increase of only 2.2 times. By comparing SEM images both before and after evaluation with the corresponding chemisorption values before and after evaluation, we have found that considerable fouling occurs for Ag particles smaller than 80 – 90 nm, making it difficult to determine the intrinsic activities of these smaller particles. The sintering and potential fouling of Ag particles during evaluation make it critical to perform SEM and selective chemisorption analyses not only for fresh catalysts, but particularly spent

catalysts, since this better represents the state of the catalyst when TOF values are determined.

Selectivity to EO, which is independent of TOF, shows the greatest sensitivity to particle size.

For Ag particles <100 nm, the intrinsic EO selectivity, defined as EO selectivity at 0.0% EO concentration where no consecutive EO combustion occurs) is ~60%, while for Ag particles >150 nm, the value is ~75%. Thus, the selectivity trends track well with fouling characteristics and, by extension, the transition from strongly-bound, nucleophilic Ag-O on smaller Ag particles to more loosely-bound, electrophilic Ag-O surface species on the larger Ag particles.

Interestingly, the TOF values and intrinsic EO selectivity for unpromoted 12 wt% Ag/α-Al_2O_3 agree very well with the Ag catalysts prepared and evaluated in this study, indicating the relevance of the results in this study to realistic EO catalysts.

Declaration of Competing Interest

The authors declare that they have no known competing financial interests or personal relationships that could have appeared to influence the work reported in this paper.

Acknowledgements

The authors gratefully acknowledge financial support from the DOE/AICHE RAPID Process Intensification Institute under DE-EE0007888 Program Code 8.9 and the NSF for funding though the Center for Rational Catalyst Synthesis, an Industry/University Cooperative Research Center under grant IIP1464595. The authors would also like to acknowledge our undergraduate assistant Jacob Stiles for his rigor in generating particle size histograms.

Appendix A. Supplementary material

Supplementary data to this article can be found online at https://doi.org/10.1016/j.jcat.2022.03.021.

References

[1] TechNavio, Global Ehtylene Oxide and Ethylene Gycol Market 2016–2020, 2016.
[2] A. Anderson, M. Motloung, Sasol Achieves Beneficial Operation of Second Lake Charles Chemicals Project Production Facility, 2019.
[3] R. Siegfried, M. Dieter, Ethylene Oxide, Wiley-VCH (Ed.) Ullmann's Encyclopedia of Industrial Chemistry, Wiley, 2012, pp. 547–571.
[4] T.E. Lefort, Process for the production of ethylene oxide, US Patent No. 1998878, 1931.
[5] H.V. Milligen, B. VanderWilp, G.J. Wells, Enhancements in the ethylene oxide/ethylene glycol manufacturing technology, in: Whitepaper, Shell Global Solutions, 2016.
[6] A.M. Lauritzen, Ethylene oxide catalyst and process for preparing the catalyst, US Patent No. 4761394, 1988.
[7] A.M. Lauritzen, Ethylene oxide catalyst process and preparing the catalyst, US Patent No. 4766105, 1988.
[8] K. Tanabe, Solid Acids and Bases, Academic Press, New York, NY, 1975, pp. 45–58.
[9] J.R. Anderson, Structure of Metallic Catalysts, Academic Press, New York, NY, 1975.
[10] K. Punyawudho, D.A. Blom, J.W.V. Zee, J.R. Monnier, Comparison of different methods for determinination of Pt surface site concentrations for supported Pt electrocatalysts, Electro. Acta 55 (2010) 5349–5356.
[11] W. Medlin, J.R. Monnier, Particle size distribution of 13.4wt% Ag supported on alpha alumina, Unpublished work, 1997.
[12] D.E. Strohmayer, G.L. Geoffroy, M.A. Vannice, Measurment of silver surface area by H_2 titration of chemisorbed oxygen, Appl. Catal. 7 (1983) 189–198.
[13] S.R. Seyedmonir, D.E. Strohmayer, G.L. Geoffroy, M.A. Vannice, Characterization of supported silver catalysts I. Adsorption of O_2, N_2, N_2O and the H_2-Titration of adsorbed oxygen on well dispersed Ag on TiO, J. Catal. 87 (1984) 424–436.
[14] B. Egelske, M. Rahman, J.R. Monnier, Hydrogen titration of oxygen precovered Ag for ethylene oxide catalysts containing common promoters and co-promoters, 2021 (in preparation).
[15] X.E. Verykios, F.P. Stein, R.W. Coughlin, Influence of metal crystallite size and mophology on selectivity and activity of ethylene oxidation catalyzed by supported silver, J. Catal. 66 (1980) 368–382.
[16] J.K. Lee, X.E. Verykios, R. Pitchai, Support and crystallite size effects in ethylene oxidation catalysis, Appl. Catal. 50 (1989) 171–188.
[17] V.Y. Gavrilov, R.A. Byanov, N.N. Bobrov, Standardization of methods apparatusses and devices for the control over commercial catalysts quality, in: Proc. USSR Symp (in Russian), 1991.
[18] J.E. van den Reijen, S. Kanungo, T.A.J. Welling, M. Versluijs-Helder, T.A. Nijhuis, K.P. de Jongh, P.E. de Jongh, Preparation and particle size effects of Ag/α-Al_2O_3 catalysts for ethylene epoxidation, J. Catal. 356 (2017) 65–74.
[19] A.J.F. van Hoof, E.A.R. Hermans, A.P. van Bavel, H. Friedrich, E.J.M. Hensen, Structure sensitivity of silver-catalyzed ethylene epoxidation, ACS Catal. 9 (2019) 9829–9839.
[20] W. Diao, J.M. Tengco, A.M. Gaffney, J.R. Regalbuto, J.R. Monnier, Rational synthesis of bimetalic catalysts using electroless deposition methods, in: J. Spivey, Y.F. Han, D. Shekhawat (Eds.), Catalysis, Royal Society of Chemistry, 2020, pp. 116–150.
[21] T.H. James, The Therory of the Photographic Process, Eastman Kodak Co, Rochester, NY, 1977.
[22] W. Diao, C.D. DiGiulio, M.T. Schaal, S. Ma, J.R. Monnier, An investigation on the role of Re as a promoter in Ag Cs Re/α-Al2O3 high-selectivity, ethylene epoxidation catalysts, J. Catal. 322 (2015) 14–23.
[23] S.N. Goncharov, B.S. Bal'zhinimaev, S.V. Tsybulya, V.I. Zaikovskii, A.F. Danilyuk, Synthesis of silver supported catalysts with narrow particle size distribution, Prepar. Catal. VI (1995) 915–922.
[24] H.J. Ploehn, J.R. Monnier, X. Chen, Systems and methods for measurement of gas permeation through polymer films, US Patent No. 8424367, 2009.
[25] J.R. Monnier, J.L. Stavinoha, G.W. Hartley, Effects of chlorine and chlorine dynamics during silver-catalyzed epoxidation of butadiene, J. Catal. 226 (2004) 321–333.
[26] J.R. Lockemeyer, R.C. Yeates, D. Reinalda, Method for improving the selectivity of a catalyst and the process for the epoxidation of an olefin, US Patent No. 8148555, 2012.
[27] N. Rizkalla, A. Rokieki, Method for making a highly selective ethylene oxide catalyst, US Patent No. 8883675, 2014.
[28] J.R. Lockemeyer, R.C. Yeates, D. Reinalda, Method for improving the selectivity of a catalyst and process for the epoxidation of an olefin, US Patent No. 7485597, 2009.
[29] W.E. Evans, J.R. Lockemeyer, D.M. Rekers, A.J.T. Raa, T. Wermink, Method for the start-up of an epoxidation process and a process for the epoxidation of an olefin, US Patent No. 7102022, 2006.
[30] J.T. Jankowiak, M.A. Barteau, Ethylene epoxidation over silver and copper-silver bimetallic catalysts: I. Kinetics and selectivity, J. Catal. 236 (2005) 366–378.
[31] K.E. Hayes, The role of reaction products in the silver-catalyzed oxidation of ethylene, Can. J. Chem. 38 (1960) 2256–2268.
[32] M. Schaal, A. Pickerell, C. Williams, J. Monnier, Characterization and evaluation of Ag–Pt/SiO catalysts prepared by electroless deposition, J. Catal. 254 (2008) 131–143.
[33] S.S. Djokic, P.L. Cavallotti, Electroless depostion: theory and applications, in: S. Science (Ed.), Electrodeposition, Springer, New York, NY, 2010, pp. 251–289.
[34] I. Ohno, Electrochemistry of electroless plating, Mat. Sci. Eng. 146 (1991) 33–49.
[35] G. Tate, A. Kenvin, W. Diao, J.R. Monnier, Preparation of Pt-containing bimetallic and trimetallic catalysts using continuous electroless deposition methods, Catal. Today 334 (2019) 113–121.
[36] B.T. Egelske, J.M. Keels, J.R. Monnier, J.R. Regalbuto, An analysis of electroless deposition derived Ni-Pt catalysts for the dry reforming of methane, J. Catal. 381 (2020) 364–384.
[37] S. PAK, Silver impregnation method for producing ethylene oxide catalyst with enhanced catalytic ability, US Patent No. 20180201595, 2018.
[38] S. Eskandari, Y. Li, F.F. Tao, J.R. Regalbuto, The use of salts to control silica supported Pt particle size in charge enhanced dry impregnation syntheses, Catal. Today 334 (2019) 187–192.
[39] A.K. Datye, Q. Xu, K.C. Kharas, J.M. McCarty, Particle size distributions in heterogeneous catalysts: what do they tell us about the sintering mechanism?, Catal Today 111 (2006) 59–67.
[40] A.J.F. van Hoof, R.C.J. van der Poll, H. Friedrich, E.J.M. Hensen, Dynamics of silver particles durring ethylene epoxidation, Appl. Catal. B 272 (2020).
[41] J.C. Wu, P. Harriott, The effect of crystallite size on the activity and selectivity of silver catalysts, J. Catal. 39 (1975) 395–402.
[42] P. Harriott, The oxidation of ehtylene using silver on different supports, J. Catal. 21 (1971) 56–65.
[43] S.N. Goncharova, E.A. Paukshtis, B.S. Bal'zhinimaev, Size effect in ethylene oxidation on silver catalysts. Influence of support and Cs promoter, Appl. Catal. A 126 (1995) 67–84.
[44] R.V. Hardeveld, F. Hartog, The statistics of surface atoms and surface sites on metal crystals, Surf. Sci. 15 (1969) 189–230.
[45] D.J. Sajkowski, M. Boudart, Structure sensitivity of the catalytic oxidation of ethene by silver, Catal. Rev. 29 (1987) 325–360.
[46] J.R. Monnier, The selective epoxidation of non-allylic olefins over supported silver catalysts, in: 3rd World Congress on Oxidation Catalysis, 1997, pp. 135–149.
[47] V. Bukhtiyarov, A. Nizovskii, H. Bluhm, M. Havecker, E. Kleimenov, A. Knopgericke, R. Schlogl, Combined in situ XPS and PTRMS study of ethylene epoxidation over silver, J. Catal. 238 (2006) 260–269.

[48] T.E. Jones, T.C. Rocha, A. Knop-Gericke, C. Stampfl, R. Schlogl, S. Piccinin, Thermodynamic and spectroscopic properties of oxygen on silver under an oxygen atmosphere, Phys. Chem. Chem. Phys. 17 (2015) 9288–9312.
[49] K.C. Waugh, M. Hague, The detailed kinetics and mechanism of ethylene epoxidation on an oxidised Ag/α-Al_2O_3 catalyst, Catal. Today 157 (2010) 44–48.
[50] W. Shen-Wu, Oxidation of ehtylene to ethylene oxide, Ind. Eng. Chem. 45 (1953) 234–238.
[51] R.E. Kenson, M. Lapkin, Kinetics and mechanism of ehtylene oxidation. Reactions of ethylene and ethylene oxide on a silver catalyst, J. Phys. Chem. 74 (1970) 1493–1502.
[52] A. Verman, S. Kaliaguine, Estimation of rate coefficients from pulsed microcatalytic reactors: oxidation of ethylene over silver catalyst, J. Catal. 30 (1973) 430–437.
[53] C.J. Chen, J.W. Harris, A. Bhan, Kinetics of ethylene epoxidation on a promoted Ag/α-Al_2O_3 catalyst – the effects of product and chloride co-feeds on rates and selectivity, Chemistry 24 (2018) 12405–12415.
[54] X.C. Guo, R.J. Madix, Adsorption of oxygen and carbon dioxide on cesium-reconstructed Ag(110) surface, Surf. Sci. 550 (2004) 81–92.
[55] M.V. Badani, M.A. Vannice, Effects of cesium chloride and oxygen adsorption on promoted Ag/α-Al_2O_3 catalysts, Appl. Catal. A 204 (1999) 129–142.
[56] C. Guckel, Ethylene oxide catalyst with optimized cesium content, US Patent No. 9115104, 2015.
[57] Y. Jun, D. Jingfa, Rhenium as a promoter for ethylene epoxidation, Appl. Catal. 92 (1992) 73–80.
[58] T. Pu, H. Tian, M.E. Ford, S. Rangarajan, I.E. Wachs, Overview of selective oxidation of ethylene to ethylene oxide by Ag catalysts, ACS Catal. 9 (2019) 10727–10750.